The modular mechanism of chromocenter formation in *Drosophila*

Madhav Jagannathan[1,*], **, Ryan Cummings[1,3,*] and Yukiko M. Yamashita[1, 2, 3,**]

1. Life Sciences Institute
2. Department of Cell and Developmental Biology
3. Howard Hughes Medical Institute,
4. University of Michigan Ann Arbor, MI 48109, USA

*: equal contributions

**: corresponding authors, madhavj@umich.edu, yukikomy@umich.edu

Abstract

A central principle underlying the ubiquity and abundance of pericentromeric satellite DNA repeats in eukaryotes has remained poorly understood. In our previous study (Jagannathan et al., 2018), we proposed that the interchromosomal clustering of satellite DNAs into nuclear structures known as chromocenters ensures encapsulation of all chromosomes into a single nucleus. Chromocenter disruption led to micronuclei formation, resulting in cell death. Here we show that chromocenter formation is mediated by a 'modular' network, where interactions between two sequence-specific satellite DNA-binding proteins, D1 and Prod, bound to their cognate satellite DNAs, bring the full complement of chromosomes into the chromocenter. *D1 prod* double mutants die during embryogenesis, exhibiting enhanced phenotypes associated with chromocenter disruption, revealing the universal importance of satellite DNAs and chromocenters. Taken together, we propose that interactions between chromocenter modules, consisting of satellite DNA binding proteins and their cognate satellite DNA, package the *Drosophila* genome within a single nucleus.

Introduction

Satellite DNAs are abundant tandem repeats that are ubiquitously found at centromeric and pericentromeric heterochromatin of eukaryotic chromosomes. Although the role of satellite DNA in centromeric heterochromatin in kinetochore function is well established (Sun et al., 1997, 2003; Willard, 1990), the role of pericentromeric heterochromatin has been obscure despite its abundance that surpasses far beyond centromeric heterochromatin. Due to the lack of protein-coding ability and lack of conservation among species, satellite DNA has been repeatedly consigned to the status of genomic junk (Ohno, 1972; Orgel and Crick, 1980), even though they can constitute ~50% of eukaryotic genomes. Although satellite DNAs have been proposed to function in diverse cellular processes such as meiotic disjunction (Dernburg et al., 1996; Hawley et al., 1992), dosage compensation (Menon et al., 2014) and chromosome segregation (Rošić et al., 2014), these functions have often been restricted to specific satellite DNA repeats, cell types or organisms. Accordingly, a central principle underlying the ubiquity and abundance of satellite DNA in eukaryotes has remained poorly understood.

In a recent study using *Drosophila* and mouse cells as models, we have proposed a conserved function of satellite DNAs in maintaining the entire chromosomal complement in a single nucleus (Jagannathan et al., 2018). Our study indicated that pericentromeric satellite DNAs play a critical role in bundling multiple chromosomes, leading to the formation of 'chromocenters', cytological structures that have been recognized for ~100 years (Figure 1A) (Jones, 1970; Jost et al., 2012; Pardue and Gall, 1970). We have shown that *Drosophila melanogaster* D1 and the mouse HMGA1 bundle chromosomes by binding to their cognate satellite DNAs ($\{AATAT\}_n$ and major satellite, respectively) and clustering them into chromocenters. Loss of chromocenters (i.e. defective bundling of chromosomes) due to mutation/depletion of these satellite DNA-binding proteins resulted in the formation of micronuclei, because unbundled chromosomes budded out of interphase nuclei. This was associated with extensive DNA damage, as has been observed with micronuclei in other systems (Crasta et al., 2012; Denais et al., 2016; Hatch et al., 2013; Raab et al., 2016). Based on these observations,

we proposed that chromocenter formation, supported by interchromosomal bundling, secures the full complement of chromosomes within a single nucleus.

Our previous study raised a few key questions. First, although some species such as mouse have the same pericentromeric satellite DNA repeat (i.e. major satellite) on all chromosomes, other species such as humans, *Drosophila*, cows and kangaroo rats are known to have divergent pericentromeric satellite DNA sequences on each chromosome (John and Miklos, 1979), raising the question as to how all chromosomes are bundled into chromocenters. For example, in *Drosophila melanogaster*, the $\{AATAT\}_n$ satellite is abundant on X, Y and 4th chromosomes (Figure 1B), and we have shown that the D1 protein, which recognizes this satellite DNA, plays a critical role in chromocenter formation. However, chromosome 2 possesses little if any of the $\{AATAT\}_n$ satellite DNA (Figure 1B, arrowheads), and chromosome 3 possesses much less of this satellite DNA compared to X, Y and 4th chromosomes (Figure 1B, arrows). Therefore, how chromosomes 2 and 3 (hereafter referred to as the major autosomes) may participate in chromocenter formation remained unclear. Second, it is widely observed that most eukaryotic cells contain multiple chromocenters, recognized as DAPI-dense foci or the association of pericentromeric satellite DNA. However, our model for chromocenter function necessitates the bundling of all chromosomes together, but how multiple chromocenter foci can mediate the bundling of all chromosomes remained unclear.

Here we show that the *Drosophila melanogaster* major autosomes are incorporated into chromocenters by the Proliferation disrupter (Prod) satellite DNA-binding protein and its cognate $\{AATAACATAG\}_n$ satellite DNA. Loss of Prod resulted in phenotypes similar to those of *D1* mutant with a different spectrum of affected tissues: defective chromocenters, micronuclei formation and loss of cellular viability in the imaginal discs and lymph glands. We show that dynamic and mutually dependent interactions between D1 and Prod mediate a network-like configuration for chromocenters, ensuring effective bundling of all *Drosophila* chromosomes. Moreover, a double mutant of *D1* and *prod* resulted in embryonic lethality with defective embryos exhibiting a striking increase in micronuclei, revealing the essential function of

chromocenters and satellite DNAs for cell viability. Taken together, we propose that modules of satellite DNA and satellite DNA-binding proteins form chromocenters, which bundle the full complement of an organism's chromosomes in a single nucleus.

Results

The {AATAACATAG}$_n$ satellite DNA-binding protein, Prod, is important for chromocenter formation.

Our previous study demonstrated that the *Drosophila* D1 protein, which binds to the {AATAT}$_n$ satellite DNA, plays a critical role in bundling chromosomes into chromocenters, such that they are encapsulated within a single nucleus. Puzzlingly, little if any{AATAT}$_n$ satellite DNA is present on 2nd chromosomes (Figure 1B), raising a question as to how these autosomes may be incorporated into chromocenters.

The {AATAACATAG}$_n$ satellite DNA drew our attention, because it is abundantly present on chromosomes 2 and 3 (Figure 1B) and is known to be bound by the Proliferation disrupter (Prod) protein (Török et al., 1997, 2000; Platero et al., 1998). Indeed, we observed that the {AATAACATAG}$_n$ satellite DNA and Prod protein perfectly co-localized within interphase nuclei in multiple cell types such as spermatogonia, imaginal disc cells and lymph gland cells (Figure 1C-E). Whereas the {AATAACATAG}$_n$ satellite DNA exists at 4 loci in diploid cells (2 from 2nd, 2 from 3rd) (Figure 1B), we predominantly observed two {AATAACATAG}$_n$ satellite DNA foci per nucleus (Figure 1C-E), suggesting that this satellite DNA is bundled into chromocenters. The number of {AATAACATAG}$_n$ satellite DNA foci per nucleus significantly increased in cells depleted of Prod (both loss-of-function mutants and RNAi) (Figure 1F-K and Figure 2 – figure supplement 1A-B), suggesting that Prod functions to bundle {AATAACATAG}$_n$ satellite DNA into chromocenters.

prod mutant cells exhibit cellular phenotypes associated with chromocenter disruption, leading to larval lethality

Loss-of-function of *prod* was reported to cause late larval lethality with these mutants containing atrophied imaginal discs and melanized lymph glands (Török et al., 1997). However, the cellular phenotypes in these degenerate tissues have not been investigated in detail. Because we observed defective chromocenter formation in *prod*

mutant imaginal discs cells (Figure 1F-H), we wondered if larval lethality may be explained by cellular defects due to chromocenter disruption.

Our prior study showed that disruption of chromocenter formation in *D1* mutants led to micronuclei formation due to lack of chromosome bundling in interphase nuclei, leading to a loss of cellular viability in the *Drosophila* germline (Jagannathan et al., 2018). Similar to these observations with *D1* mutant cells, we observed that mutation of *prod* resulted in the formation of micronuclei in larval imaginal discs (Figure 2A-B, E) and lymph glands (Figure 2C-E). These micronuclei almost always contained satellite DNA (Figure 2F, >80% of micronuclei contained at least one of $\{AATAT\}_n$ or $\{AATAACATAG\}_n$ satellite DNAs (n=48)), supporting the idea that micronuclei formation is due to declustering of chromocenters.

It is well established that the DNA within micronuclei is prone to genomic instability including excessive levels of DNA damage (Crasta et al., 2012; Hatch et al., 2013). We have shown that this is the case with *D1* mutant germ cells in *Drosophila*, leading to cell lethality (Jagannathan et al., 2018). We therefore quantified cells containing DNA damage assessed by anti-γ-H2Av antibody staining in *prod* mutant imaginal discs and lymph glands. We did not observe a significant difference in DNA damage levels between heterozygous control and *prod* mutant tissues (control imaginal disc cells – 0%, n=161, *prod* mutant imaginal disc cells – 1.9%, n=159, control lymph gland cells – 0.7%, n=280 and *prod* mutant lymph gland cells – 1.4%, n=143). However, when apoptotic cell death was blocked by expressing the death-associated inhibitor of apoptosis 1 (DIAP1) protein (Orme and Meier, 2009), we observed a striking increase in DNA damage in *prod* mutant tissues (Figure 2G-J), suggesting that *prod* mutation indeed increases DNA damage and that these damaged cells are rapidly cleared by apoptosis. Taken together, these results suggest that micronuclei formation in *prod* mutant tissues arising from chromocenter disruption leads to cell death due to elevated DNA damage, thereby resulting in the atrophy of essential somatic tissues and thus larval lethality.

We previously showed that *D1* mutation mainly affected germ cells (Jagannathan et al., 2018). To examine the role of *prod* in germ cells, we used RNAi-mediated knockdown (Figure 2 – figure supplement 1A-B) and loss-of-function clones (Figure 2 – figure supplement 1C-D). Germline depletion of *prod* resulted in disruption of $\{AATAACATAG\}_n$ satellite DNA clustering (Figure 1I-K) and defects in nuclear integrity: 27.9 % of *prod*-depleted germ cells (n=190) exhibited leakage of nls-GFP in comparison to 3.7% of control cells (n=191) (Figure 2 – figure supplement 1E-F). However, we did not observe a dramatic loss of germ cell viability (Figure 2 – figure supplement 1A-D, G) or an increase in micronuclei formation in *prod*-depleted testes (no micronuclei were observed in both control and $prod^{RNAi}$ cells, n=200 in both conditions). Conversely, *D1* mutation, which results in severe micronuclei formation and cell death in the germline, did not show a significant increase in micronuclei formation in somatic tissues that are affected by *prod* mutation such as imaginal discs and lymph glands (Figure 2 - figure supplement 2A-C). These results show that while both *D1* and *prod* are important chromocenter-forming proteins, their depletion affects distinct tissues. Despite the distinct tissue requirement of these genes, *D1 prod* double mutant exhibited synthetic lethality (see below) suggesting that these genes function in the same biological process. At the moment, the underlying cause(s) of tissue specificity remain elusive although it is possible that tissue-specific nuclear organization may make each cell type more or less sensitive to the perturbation of X-Y-4 chromosome bundling vs. major autosome bundling.

Ectopic expression of Prod bundles heterologous chromosomes in spermatocytes.

The above results show that Prod, like D1, plays a critical role in chromocenter formation. Based on our previous observation that D1 protein forms 'chromatin threads' that connect heterologous chromosomes (Jagannathan et al., 2018), we postulated that these chromatin threads are the basis for chromocenter formation. Similarly, we observed chromatin threads with Prod protein (Figure 3A, arrowheads indicate two of the four Prod loci while the arrow indicates Prod threads connecting the two loci). However, these D1/Prod-positive chromatin threads are only apparent during a narrow time window during mitotic prophase when individual chromosomes start to resolve from each other

during chromosome condensation but prior to metaphase. By metaphase, the chromatin threads that connect heterologous chromosomes were completely resolved, likely to allow mitotic chromosome segregation. Accordingly, it has been challenging to visualize the clustering of heterologous chromosomes within chromocenters during interphase.

Strikingly, we found that ectopic expression of Prod in spermatocytes, which normally lack Prod (Figure 3 - Figure supplement 1), led to the formation of chromatin threads between heterologous chromosomes. It is well established that homologous chromosomes separate into distinct 'territories' within the nucleus in preparation of meiotic reductional division in spermatocytes of *Drosophila* (Figure 3B) (McKee, 2004). Ectopic expression of GFP-tagged Prod protein in spermatocytes resulted in the formation of chromatin threads between distinct chromosome territories (Figure 3C) with these bridges positive for both Prod protein and the $\{AATAACATAG\}_n$ satellite DNA (Figure 3C, arrows indicate Prod-$\{AATAACATAG\}_n$ threads connecting chromosome territories marked by the yellow dashed lines). The two chromosomal territories connected by ectopically expressed Prod are territories containing chromosomes 2 and 3, as determined by FISH using 2nd and 3rd chromosome specific probes ($\{AACAC\}_n$ satellite for 2, dodeca satellite for 3) (Figure 3D). These data clearly demonstrate that ectopically expressed Prod bound the $\{AATAACATAG\}_n$ satellite DNA on chromosomes 2 and 3, and physically linked these chromosomes. We conclude that Prod is sufficient to bundle heterologous chromosomes via binding its cognate satellite DNA, $\{AATAACATAG\}_n$, providing a mechanistic explanation how chromocenters are formed by bundling of specific satellite DNA sequences located on heterologous chromosomes.

D1 and Prod foci dynamically associate in interphase nuclei.

The results described above and our previous study establish that D1 and Prod are required to cluster pericentromeric satellite DNAs to form chromocenters. D1 and Prod each bundle chromosomes that contain their cognate satellite DNA. However, this raises the question as to how the entire set of chromosomes can be bundled together such that they are encapsulated in the same nucleus. We noted that D1 and Prod were predicted to

interact with each other, albeit weakly, based on a high-throughput mass spectrometry screen in Schneider S2 cells (Guruharsha et al., 2011), suggesting that satellite DNA bundled by D1 and that bundled by Prod might further cluster together via an interaction between Prod and D1 proteins. However, co-immunoprecipitation experiments did not detect any physical interaction between these proteins (Figure 4 - figure supplement 1), suggesting that their interaction may be weak or transient. We observed that D1- and Prod-positive foci were consistently juxtaposed within the heterochromatic domain of the nucleus (Figure 4A, the heterochromatic domain is demarcated by the yellow dashed line and is based on HP1 localization). This pattern of D1 and Prod localization was observed in multiple cell types (Figure 4 – figure supplement 2A-C, arrows indicate juxtaposed foci). Based on the weak interaction detected by immunoprecipitation/mass-spectrometry and juxtaposition of D1 and Prod foci within the nucleus, we hypothesized that the interaction of D1 and Prod may be transient.

To examine this possibility, we conducted time-lapse live observation by combining GFP-D1 and mCherry-Prod expressed in spermatogonial cells. While we have observed an average of ~4-5 D1-positive foci/nucleus and ~2 Prod positive foci/nucleus in fixed and stained samples, the live observation demonstrated that these foci are not static but rather moving dynamically within the nucleus (Figure 4B-C and supplementary movie 1). Using single particle tracking, we estimated the diffusion coefficient (D), which indicated that D1 and Prod exhibited similar dynamics (Figure 4D). We also quantified the slope of momentum scaling spectrum (S_{MSS}) of D1 and Prod foci, an established parameter for the type of particle movement (Ewers et al., 2005). In the case of free, unhindered diffusion, the S_{MSS} value equals 0.5 whereas values below and above 0.5 indicate confined and directed motion respectively. The majority of D1 and Prod foci exhibit $S_{MSS} < 0.5$ (Figure 4E), suggesting confined motion, likely within the heterochromatin domain. D1-positive foci and Prod-positive foci interacted in a ‘kiss and run’ manner: coming into contact temporarily and separating from each other soon after (Figure 4F-G). These results indicate that chromocenter is a structure comprised of dynamic modules of satellite DNAs and satellite DNA binding proteins, rather than rigidly linked satellite DNAs. The dynamism exhibited by these satellite DNA binding

proteins may reflect the recently demonstrated liquid droplet-like properties of heterochromatin (Larson et al., 2017; Strom et al., 2017).

The frequent associations of D1 and Prod led us to examine whether these modules may exhibit inter-dependency in chromocenter formation. Indeed, we found that mutation of *prod* resulted in defective clustering of D1 protein within the nuclei of imaginal discs, neuroblasts and spermatogonial germ cells (Figure 4H-J and Figure 4 – figure supplement 2D-I). Similarly, mutation of *D1* resulted in the disruption of Prod protein clustering in multiple tissues (Figure 4K-M and Figure 4 – figure supplement 2J-O). Taken together, these results support the idea that modules of Prod, D1 and their cognate satellite DNA function in a mutually dependent manner to form chromocenters. We propose that this inter-dependency shapes a network-like configuration for chromocenters and forms the basis for bundling the 'entire set' of chromosomes, instead of bundling individual satellite DNAs.

D1 prod double mutant exhibits embryonic lethality

While our data suggest that both D1 and Prod play a role in chromocenter formation, loss of either protein only resulted in tissue-specific cellular defects. To test the possibility that D1 and Prod might have partly redundant functions, we examined the development of *D1 prod* double mutants using loss-of-function alleles ($prod^{k08810}$/CyO, Act-GFP; $D1^{LL03310}$/TM3, Act-GFP). As wild type alleles of *prod* and *D1* were carried on the balancer chromosomes marked by GFP expression, only the double mutant animals are GFP-negative, whereas any animal that carries at least 1 wild-type allele of *D1* or *prod* are GFP-positive. We observed that *D1* and *prod* double mutants (i.e. GFP-negative animals) were underrepresented (far below expected frequency at 6.25%) in larval population in contrast to GFP-negative larvae from control parents (+/CyO, Act-GFP; +/TM3, Act-GFP) (Figure 5A). These data suggested that double mutant animals largely failed to develop past the embryo stage.

A closer examination revealed that 7.6% of embryos from mated *D1* and *prod* heterozygote parents exhibited abnormal development, (Figure 5C). This number closely

matches with the expected frequency of 6.25% for double mutant embryos. We observed micronuclei in these defective embryos (Figure 5D-E) as well as numerous extranuclear DAPI-intense foci (Figure 5E, arrows), which we suggest is the terminal phenotype of cells with micronuclei due to chromocenter disruption. Taken together, our data establish the critical requirement of chromocenters and satellite DNA in maintaining the entire genome in a single nucleus and supporting cellular viability.

Discussion

Satellite DNAs are one of the most abundant and ubiquitous elements of eukaryotic genomes. Nevertheless, these tandem repeats have often been dismissed as 'junk' DNA for the following reasons, (a) they are simple sequences with no apparent protein coding potential, (b) there is a striking lack of conservation in the abundance and identity of satellite DNA repeats even amongst closely related species. Nonetheless, satellite DNA abundance is remarkably stable over multiple generations, despite being prone to copy number loss through mechanisms such as replicative slippage and intrachromatid exchange (Charlesworth et al., 1994), implying that satellite DNA must serve unappreciated function(s).

We have recently proposed a conserved function for pericentromeric satellite DNAs in encapsulating the entire chromosomal complement within a single nucleus (Jagannathan et al., 2018). The framework of this model is that satellite binding proteins, *Drosophila melanogaster* D1 and mouse HMGA1, bind their cognate satellite DNAs and bundle them into chromocenters. This bundling prevents individual chromosomes from budding off out of the nucleus, thereby maintaining chromosomes within the nucleus. Based on this idea, all the chromosomes must be bundled into chromocenters so as not to be lost as micronuclei. This raised a few questions. 1) How can all of the *D. melanogaster* chromosomes be bundled into chromocenters, given that the D1-bound $\{AATAT\}_n$ satellite DNA is present abundantly only on X,Y& 4^{th} chromosomes? and 2) If bundling of all chromosomes into chromocenters is required to package the genome into a single nucleus and given the multiple chromocenter foci typically observed in *Drosophila* and mouse cells, are these chromocenters linked to one another? In this study, through the investigation of Prod protein in *Drosophila melanogaster*, we provide insights into these questions.

First, we found that Prod, which is known to bind the $\{AATAACATAG\}_n$ satellite DNA on the major autosomes, is a chromocenter-forming protein, functioning together with D1 protein. Our study suggests that the chromocenter consists of multiple modules of satellite DNAs and satellite DNA-binding proteins, where D1 bundles X, Y &

4th chromosomes and Prod bundles 2nd and 3rd chromosomes, thereby covering the full complement of the chromosomes (Figure 5F). Given that the *Drosophila melanogaster* genome contains at least 17 satellite DNAs (Jagannathan et al., 2017; Lohe et al., 1993) , it is plausible that additional satellite DNA binding proteins may participate in chromocenter formation, even though D1 and Prod can cover the full complement of *D. melanogaster* chromosomes. Alternatively, these 17 satellite DNAs might reflect the history of the species, wherein individual satellites were essential at some point, while only a subset are critically important for the present day *D. melanogaster* genome.

We observed that D1-positive foci and Prod-positive foci dynamically interacted within the interphase nuclei. Moreover, D1 and Prod function interdependently such that D1/$\{AATAT\}_n$ clustering is dependent on Prod while Prod/$\{AATAACTAG\}_n$ clustering is dependent on D1. We suggest that these interactions between satellite DNA binding proteins can form a chromocenter network, thereby packaging the entire genome within a single nucleus. Importantly, while mutation of either *D1* or *prod* exhibited varying effects on micronuclei formation in a tissue-specific manner, a *D1 prod* double mutant resulted in a striking enhancement of the phenotype, leading to embryonic lethality. This suggests that while cells can compensate for the loss of an individual chromocenter module, loss of multiple chromocenter modules will result in more widespread and penetrant cellular defects, illuminating an essential function for chromocenter formation.

Our data suggest that the essence of satellite DNA function is to be bound by sequence-specific binding proteins that have the ability to bundle these repeats into chromocenters. As such, the satellite DNA sequence itself does not need to be conserved. This may explain why satellite DNA repeats diverge rapidly, even among closely related species, an observation that has led to the idea that satellite DNA is junk. For instance, the $\{AATAACATAG\}_n$ satellite DNA, which is a central player in bundling the *Drosophila melanogaster* major autosomes, is completely absent in its nearest relative, *Drosophila simulans*. These observations lead to an interesting speculation: if satellite DNA repeats diverge rapidly, their binding proteins will also likely adapt to attain optimal binding specificity for the diverged sequences. Whereas *D. melanogaster* Prod

binds the $\{AATAACATAG\}_n$ satellite DNA, *D. simulans* Prod must have adapted to bind a distinct satellite DNA sequence to form chromocenters. This leads to a question as to whether *D. melanogaster* Prod can bundle *D. simulans* chromosomes and vice versa. It is tempting to speculate that such divergence in satellite DNA sequences and their binding proteins may lead to incompatibility in chromocenter formation when chromosomes from these two species are brought together in hybrids.

In summary, we propose that satellite DNA and their binding proteins conform to a modular system, whereby all the chromosomes are brought into a chromocenter network by the interaction of satellite DNA binding proteins. In this manner, chromocenter plays a fundamental role in securing all the chromosomes within a single nucleus.

Acknowledgements

We thank Cheng-Yu Lee, Georg Krohne, Tibor Torok, Bloomington Drosophila Stock Center, Kyoto Stock Center and Developmental Studies Hybridoma Bank for reagents and resources. We thank the Yamashita lab members for discussion and comments on the manuscript. This research was supported by the Howard Hughes Medical Institute (Y.Y) and an American Heart Association postdoctoral fellowship (M.J). MJ and YY conceived the project, interpreted the data and wrote the manuscript. All authors contributed to conducting experiments and analyzing data.

Materials and Methods

Fly husbandry and strains. All fly stocks were raised on standard Bloomington medium at 25°C. The following fly stocks were used: *prod*^{U} (BDSC42686), *UAS-GFP-nls* (BDSC4776), *tub-gal4* (BDSC5128), *hs-flp* (BDSC6), *FRT42D, Ubi-nls-GFP* (BDSC5626), *UAS-dcr-2* (BDSC24650), *D1-GFP* (BDSC50850), *HP1-RFP* (BDSC30562) and *UAS-DIAP1* (BDSC6657) were obtained from the Bloomington *Drosophila* stock center. *D1*^{LL03310} (DGRC140754) and *FRT42D prod*^{k08810} (DGRC111248) were obtained from the Kyoto stock center. *UAS-prod*^{RNAi} (VDRCv106593) was obtained from the Vienna Drosophila stock center. *nos-gal4* and *bam-gal4* have been previously described (Chen and McKearin, 2003; Van Doren et al., 1998). *wor-gal4* was a kind gift from Cheng-Yu Lee. Prod-null clones (indicated by loss of GFP signal) were generated as follows – Testes from flies of the genotype *hs-flp; FRT42D, Ubi-nls-GFP/FRT42D, prod*^{k08810} were dissected 48h following a 1 hour heat shock at 37°C. For embryo and larval development analysis, flies laid eggs on apple-agar at RT and development was assessed every 24 hr.

Transgene construction. For construction of *pUASt-GFP-Prod*, the *Prod* ORF was PCR-amplified from cDNA using the following primer pair, 5'-GTAGCGGCCGCAATGAACGGCAAGATG-3' and 5'-GTAGGTACCCTATAAGGACGGCGGATCG-3'. The amplified fragment was subcloned into the NotI and KpnI sites of *pUASt-EGFP-attB* (Salzmann et al., 2013) resulting in *pUASt-GFP-Prod*. For construction of *pUASt-mCherry-Prod*, the mCherry ORF was PCR amplified from a plasmid template using the following primer pair, 5'-GTAGAATTCCATCGCCACCATGGTGAGCAAGGGCGAGGAG-3' and 5'-GTAGCGGCCGCCTTGTACAGCTCGTCCATGCC-3'. The amplified fragment was subcloned into the EcoRI and NotI sites of *pUASt-GFP-Prod*, replacing the GFP fluorophore, and resulting in *pUASt-mCherry-Prod*. Transgenic flies were generated by PhiC31 integrase-mediated transgenesis into the *attP2* site (BestGene).

Immunofluorescence staining and microscopy. For *Drosophila* tissues, immunofluorescence staining was performed as described previously (Cheng et al., 2008). Briefly, tissues were dissected in PBS, transferred to 4% formaldehyde in PBS and fixed for 30 minutes. Tissues were then washed in PBS-T (PBS containing 0.1% Triton-X) for at least 60 minutes, followed by incubation with primary antibody in 3% bovine serum albumin (BSA) in PBS-T at 4°C overnight. Samples were washed for 60 minutes (three 20-minute washes) in PBS-T, incubated with secondary antibody in 3% BSA in PBS-T at 4°C overnight, washed as above, and mounted in VECTASHIELD with DAPI (Vector Labs). For *Drosophila* embryos, 0-16h embryos were collected, dechorionated in 50% bleach, fixed and then devitellinized in methanol. The following primary antibodies were used: rabbit anti-vasa (1:200; d-26; Santa Cruz Biotechnology), mouse anti-LaminDm$_0$ (ADL84.12, 1:200, Developmental Studies Hybridoma Bank), mouse anti-γ–H2Av (UNC93-5.2.1, 1:400, Developmental Studies Hybridoma Bank), Phalloidin-Alexa546 (ThermoFisher, a22283, 1:200), rabbit anti-Prod (gift from Tibor Torok, 1:5000) and guinea pig anti-D1 (generated using the synthetic peptide CDGENDANDGYVSDNYNDSESVAA (Covance)). Images were taken using a Leica TCS SP8 confocal microscope with 63x oil-immersion objectives (NA=1.4). Deconvolution was performed when indicated using the Hyvolution package from Leica. Images were processed using Adobe Photoshop software.

Time-lapse live imaging. Testes from newly eclosed flies were dissected into Schneider's *Drosophila* medium containing 10% fetal bovine serum. The testis tips were placed inside a sterile glass-bottom chamber and were mounted on a three-axis computer-controlled piezoelectric stage. An inverted Leica TCS SP8 confocal microscope with a 63× oil immersion objective (NA = 1.4) was used for imaging. Single particle tracking was performed using the MOSAIC suite plugin for ImageJ on 0.75mm z-sections. We followed a previously established approach (Ewers et al., 2005; Siebrasse et al., 2016) to measure the dynamics of D1 and Prod foci. Both the diffusion co-efficient (D) and slope of the momentum scaling spectrum (S_{MSS}) were determined using the MOSAIC suites plugin. The MSS will show a straight line through the origin and its slope (S_{MSS}) is an

excellent measure for the type of movement. In case of free, unconstrained diffusion, the slope is 0.5 while values above and below 0.5 indicate directed motion or confined motion respectively. All images were processed using Adobe Photoshop software.

DNA fluorescence *in situ* hybridization. Whole mount *Drosophila* tissues were prepared as described above, and optional immunofluorescence staining protocol was carried out first. Subsequently, samples were post-fixed with 4% formaldehyde for 10 minutes and washed in PBS-T for 30 minutes. Fixed samples were incubated with 2 mg/ml RNase A solution at 37°C for 10 minutes, then washed with PBS-T + 1mM EDTA. Samples were washed in 2xSSC-T (2xSSC containing 0.1% Tween-20) with increasing formamide concentrations (20%, 40% and 50%) for 15 minutes each followed by a final 30-minute wash in 50% formamide. Hybridization buffer (50% formamide, 10% dextran sulfate, 2x SSC, 1mM EDTA, 1 μM probe) was added to washed samples. Samples were denatured at 91°C for 2 minutes, then incubated overnight at 37°C. For mitotic chromosome spreads, larval 3rd instar brains were squashed according to previously described methods (Larracuente and Ferree, 2015). Briefly, tissue was dissected into 0.5% sodium citrate for 5-10 minutes and fixed in 45% acetic acid/2.2% formaldehyde for 4-5 minutes. Fixed tissues were firmly squashed with a cover slip and slides were submerged in liquid nitrogen until bubbling ceased. Coverslips were then removed with a razor blade and slides were dehydrated in 100% ethanol for at least 5 minutes. After drying, hybridization mix (50% formamide, 2x SSC, 10% dextran sulfate, 100 ng of each probe) was applied directly to the slide, samples were heat denatured at 95°C for 5 minutes and allowed to hybridize overnight at room temperature. Following hybridization, slides were washed 3 times for 15 minutes in 0.2X SSC and mounted with VECTASHIELD with DAPI (Vector Labs). The following probes were used for *Drosophila* in situ hybridization: $\{AATAT\}_6$, $\{AACAC\}_6$, {dodeca}, $\{AATAACATAG\}_3$ and have been previously described (Jagannathan et al., 2017).

Immunoprecipitation. *Drosophila* testis lysate was obtained from Upd tumor testes expressing either GFP or GFP-Prod under the control of *nos-gal4* while *Drosophila* brain

lysate was obtained from third instar larval brains expressing GFP or GFP-Prod under the control of *wor-gal4*. Both sets of tissues were dissected into Schneider's *Drosophila* Medium (Thermo Fisher, 21720-024). Tissue were lysed in a buffer containing 50 mM Tris (pH 7.5), 5% glycerol, 0.2% IGEPAL, 1.5 mM $MgCl_2$, 125 mM NaCl supplemented with 1 mM PMSF and protease inhibitor cocktail (Sigma, P8340) on ice for 30 minutes. Lysates were then centrifuged at 14,000 rpm for 15 minutes at 4°C and the supernatant was incubated with GFP-Trap beads (ChromoTek, gtmak-20) for 3 hours at 4°C by rotating the tubes end-over-end. The beads were washed three times with the supplied wash buffer and boiled for 10 minutes at 95°C in 2x SDS-sample buffer to dissociate immunoprecipitated proteins from the beads.

SDS-PAGE and Western Blotting. SDS-PAGE and Western blotting were used to analyze the immunoprecipitated proteins. Samples were run on 10% Tris-glycine gels (Thermo Fisher, XP00100BOX) and subsequently transferred onto PVDF membranes (Bio-Rad, 162-0177) using the XCell II Blot Module (Thermo Fisher, EI9051). The antibodies used for Western blotting were rabbit anit-GFP (ab290, 1:7,500, abcam), guinea pig anti-D1 (1:1,000, same as above), HRP-conjugated goat anti-rabbit (1:10,000, abcam, ab97051) and HRP-conjugated goat anti-guinea pig (1:10,000, abcam, ab97155).

References

Charlesworth, B., Sniegowski, P., and Stephan, W. (1994). The evolutionary dynamics of repetitive DNA in eukaryotes. Nature *371*, 215–220.

Chen, D., and McKearin, D.M. (2003). A discrete transcriptional silencer in the bam gene determines asymmetric division of the Drosophila germline stem cell. Development *130*, 1159–1170.

Cheng, J., Türkel, N., Hemati, N., Fuller, M.T., Hunt, A.J., and Yamashita, Y.M. (2008). Centrosome misorientation reduces stem cell division during ageing. Nature *456*, 599–604.

Crasta, K., Ganem, N.J., Dagher, R., Lantermann, A.B., Ivanova, E.V., Pan, Y., Nezi, L., Protopopov, A., Chowdhury, D., and Pellman, D. (2012). DNA breaks and chromosome pulverization from errors in mitosis. Nature *482*, 53–58.

Denais, C.M., Gilbert, R.M., Isermann, P., McGregor, A.L., te Lindert, M., Weigelin, B., Davidson, P.M., Friedl, P., Wolf, K., and Lammerding, J. (2016). Nuclear envelope rupture and repair during cancer cell migration. Science *352*, 353–358.

Dernburg, A.F., Sedat, J.W., and Hawley, R.S. (1996). Direct evidence of a role for heterochromatin in meiotic chromosome segregation. Cell *86*, 135–146.

Van Doren, M., Williamson, A.L., and Lehmann, R. (1998). Regulation of zygotic gene expression in Drosophila primordial germ cells. Curr. Biol. *8*, 243–246.

Ewers, H., Smith, A.E., Sbalzarini, I.F., Lilie, H., Koumoutsakos, P., and Helenius, A. (2005). Single-particle tracking of murine polyoma virus-like particles on live cells and artificial membranes. Proc. Natl. Acad. Sci. U.S.A. *102*, 15110–15115.

Guruharsha, K.G., Rual, J.-F.F., Zhai, B., Mintseris, J., Vaidya, P., Vaidya, N., Beekman, C., Wong, C., Rhee, D.Y., Cenaj, O., et al. (2011). A protein complex network of Drosophila melanogaster. Cell *147*, 690–703.

Hatch, E.M., Fischer, A.H., Deerinck, T.J., and Hetzer, M.W. (2013). Catastrophic nuclear envelope collapse in cancer cell micronuclei. Cell *154*, 47–60.

Hawley, RS, Irick, H, and Haddox, DA (1992). There are two mechanisms of achiasmate segregation in Drosophila females, one of which requires heterochromatic homology. Developmental Genetics *13*, 440-467.

Jagannathan, M., Warsinger-Pepe, N., Watase, G.J., and Yamashita, Y.M. (2017). Comparative Analysis of Satellite DNA in the Drosophila melanogaster Species Complex. G3 (Bethesda) *7*, 693–704.

Jagannathan, M., Cummings, R., and Yamashita, Y.M. (2018). A conserved function for pericentromeric satellite DNA. Elife *26;7*. pii: e34122

John, B., and Miklos, G. (1979). Functional aspects of satellite DNA and heterochromatin. International Review of Cytology *58*, 1–114.

Jones, K.W. (1970). Chromosomal and nuclear location of mouse satellite DNA in individual cells. Nature *225*, 912–915.

Jost, K.L., Bertulat, B., and Cardoso, M.C. (2012). Heterochromatin and gene positioning: inside, outside, any side? Chromosoma *121*, 555–563.

Larracuente, A.M., and Ferree, P.M. (2015). Simple method for fluorescence DNA in situ hybridization to squashed chromosomes. J Vis Exp 52288.

Larson, A.G., Elnatan, D., Keenen, M.M., Trnka, M.J., Johnston, J.B., Burlingame, A.L., Agard, D.A., Redding, S., and Narlikar, G.J. (2017). Liquid droplet formation by HP1α suggests a role for phase separation in heterochromatin. Nature *547*, 236–240.

Lohe, A.R., Hilliker, A.J., and Roberts, P.A. (1993). Mapping simple repeated DNA sequences in heterochromatin of Drosophila melanogaster. Genetics *134*, 1149–1174.

McKee, B.D. (2004). Homologous pairing and chromosome dynamics in meiosis and mitosis. Biochim. Biophys. Acta *1677*, 165–180.

Menon, D.U., Coarfa, C., Xiao, W., Gunaratne, P.H., and Meller, V.H. (2014). siRNAs from an X-linked satellite repeat promote X-chromosome recognition in Drosophila melanogaster. Proc. Natl. Acad. Sci. U.S.A. *111*, 16460–16465.

Ohno, S. (1972). So much "junk" DNA in our genome. Brookhaven Symp. Biol. *23*, 366–370.

Orgel, L.E., and Crick, F.H. (1980). Selfish DNA: the ultimate parasite. Nature *284*, 604–607.

Orme, M., and Meier, P. (2009). Inhibitor of apoptosis proteins in Drosophila: gatekeepers of death. Apoptosis *14*, 950–960.

Pardue, M.L., and Gall, J.G. (1970). Chromosomal localization of mouse satellite DNA. Science *168*, 1356–1358.

Platero, J.S., Csink, A.K., Quintanilla, A. and Henikoff, S. (1998). Changes in chromosomal localization of heterochromatin-binding proteins during the cell cycle in Drosophila. J Cell Biol. *140(6)*, 1297-1306

Raab, M., Gentili, M., de Belly, H., Thiam, H.R., Vargas, P., Jimenez, A.J.,

Lautenschlaeger, F., Voituriez, R., Lennon-Duménil, A.M., Manel, N. and Piel, M. (2016). ESCRT III repairs nuclear envelope ruptures during cell migration to limit DNA damage and cell death. Science *352*, 359–362.

Rošić, S., Köhler, F., and Erhardt, S. (2014). Repetitive centromeric satellite RNA is essential for kinetochore formation and cell division. J. Cell Biol. *207*, 335–349.

Salzmann, V., Inaba, M., Cheng, J., and Yamashita, Y.M. (2013). Lineage tracing quantification reveals symmetric stem cell division in Drosophila male germline stem cells. Cell Mol Bioeng *6*, 441–448.

Siebrasse, J.P., Djuric, I., Schulze, U., Schlüter, M.A., Pavenstädt, H., Weide, T., and Kubitscheck, U. (2016). Trajectories and single-particle tracking data of intracellular vesicles loaded with either SNAP-Crb3A or SNAP-Crb3B. Data Brief *7*, 1665–1669.

Strom, A.R., Emelyanov, A.V., Mir, M., Fyodorov, D.V., Darzacq, X., and Karpen, G.H. (2017). Phase separation drives heterochromatin domain formation. Nature *547*, 241–245.

Sun, X., Wahlstrom, J., and Karpen, G. (1997). Molecular structure of a functional Drosophila centromere. Cell *91*, 1007–1019.

Sun, X., Le, H.D., Wahlstrom, J.M., and Karpen, G.H. (2003). Sequence analysis of a functional Drosophila centromere. Genome Res. *13*, 182–194.

Török, T., Harvie, P.D., Buratovich, M., and Bryant, P.J. (1997). The product of proliferation disrupter is concentrated at centromeres and required for mitotic chromosome condensation and cell proliferation in Drosophila. Genes Dev. *11*, 213–225.

Török, T., Gorjánácz, M., Bryant, P.J., and Kiss, I. (2000). Prod is a novel DNA-binding protein that binds to the 1.686 g/cm(3) 10 bp satellite repeat of Drosophila melanogaster. Nucleic Acids Res. *28*, 3551–3557.

Willard, H.F. (1990). Centromeres of mammalian chromosomes. Trends Genet. *6*, 410–416.

Figure 1

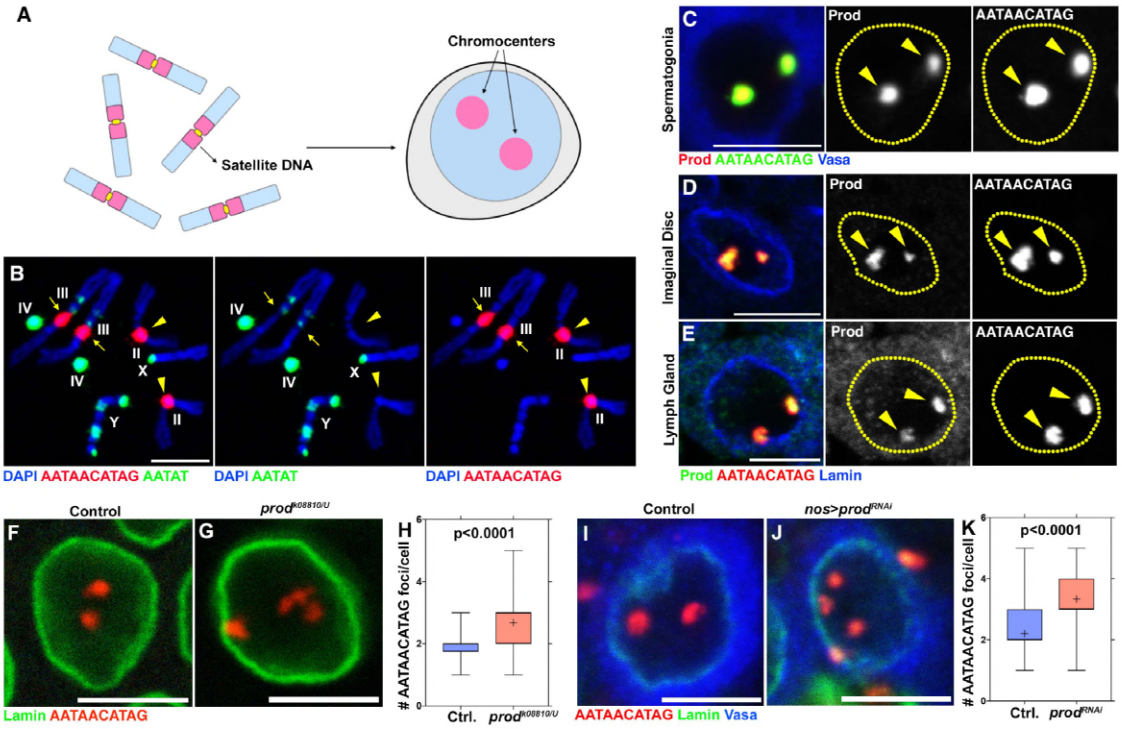

Figure 1. Prod bundles the {AATAACATAG}$_n$ satellite DNA on the *Drosophila melanogaster* major autosomes into chromocenters. (A) Schematic of chromosomes containing distinct pericentromeric satellite DNAs being organized into chromocenters. (B) FISH against the {AATAACATAG}$_n$ satellite (red) and the {AATAT}$_n$ satellite (green) on *Drosophila* larval neuroblast mitotic chromosomes co-stained with DAPI (blue) indicating the locations of these satellites in the *Drosophila* genome. (C) FISH against the {AATAACATAG}$_n$ satellite (green) in a spermatogonium co-stained with Prod (red) and Vasa (blue). (D, E) FISH against the {AATAACATAG}$_n$ satellite (green) in larval imaginal disc cells (D) and larval lymph gland cells (E) co-stained with Prod (red) and Lamin (blue). (F, G) FISH against the {AATAACATAG}$_n$ satellite (red) in heterozygous control (F) and *prod*$^{k08810/U}$ (G) larval imaginal disc cells co-stained with Lamin (green). (H) Quantification of the number of {AATAACATAG}$_n$ chromocenters per larval imaginal disc cell (heterozygous control n=70, *prod*$^{k08810/U}$ n=71). (I, J) FISH against the {AATAACATAG}$_n$ satellite (red) in control (*nos-gal4*/+; *UAS-dcr-2*/+) (I) and Prod depleted (*nos-gal4*/*UAS-prod*^{RNAi}; *UAS-dcr-2*/+) (J) spermatogonia co-stained with Lamin (green) and Vasa (blue). (K) Quantification of {AATAACATAG}$_n$

chromocenters per spermatogonium (control n=75, nos>*prod*^{RNAi} n=75). P values from Student's t-test are shown and crosshairs mark the mean. All scale bars are 5μm.

Figure 2

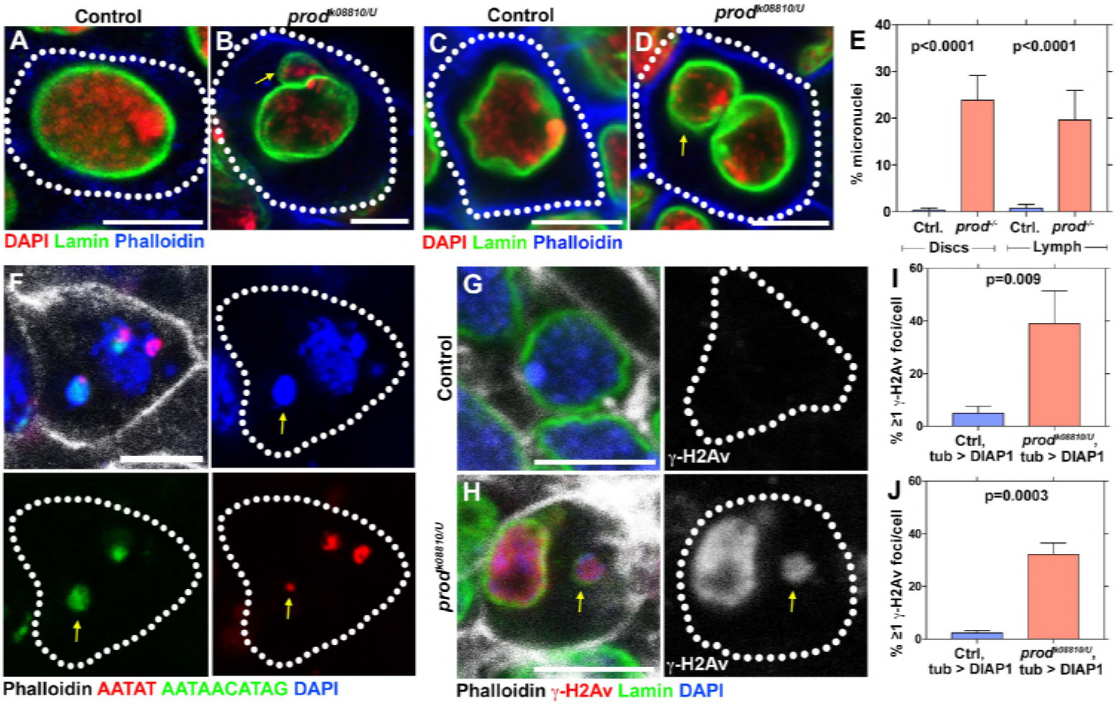

Figure 2. Loss of *prod* results in micronuclei formation and elevated DNA damage in larval imaginal discs and lymph glands. (A, B) Heterozygous control (A) and *prod*$^{k08810/U}$ mutant (B) larval imaginal disc cells stained with DAPI (red), Lamin (green), and Phalloidin (blue). Arrow indicates micronucleus. (C, D) Heterozygous control (C) and *prod*$^{k08810/U}$ mutant (D) larval lymph gland cells stained with DAPI (red), Lamin (green), and Phalloidin (blue). Arrow indicates micronucleus. (E) Quantification of micronuclei containing cells in heterozygous control and *prod*$^{k08810/U}$ mutant imaginal discs and lymph glands. Control discs n=744, *prod* mutant discs n=501, Control lymph n=664, *prod* mutant lymph n=345. (F) FISH against the $\{AATAT\}_n$ satellite (red) and the $\{AATAACATAG\}_n$ satellite (green) in a larval imaginal disc cell co-stained with Phalloidin (white) and DAPI (blue). Arrow indicates the presence of the third chromosome in the micronucleus. (G, H) Heterozygous control (G) and *prod*$^{k08810/U}$ mutant (H) larval imaginal disc cells stained with Phalloidin (white), γ-H2Av (red), Lamin (green), and DAPI (blue). Arrow indicates DNA damage in the micronucleus based on γ-H2Av staining. (I, J) Quantification of cells containing ≥1 γ-H2Av foci in heterozygous control and *prod*$^{k08810/U}$ imaginal discs (I) and lymph glands (J). In all cases,

apoptotic cell death was blocked by expressing *UAS-DIAP1* with a ubiquitous *tub-gal4* driver. Control discs n=577, *prod* mutant discs n=278, Control lymph n=330, *prod* mutant lymph n=216. P values from student's t-test are shown. All error bars: SD. All scale bars: 5μm.

Figure 2 – figure supplement 1

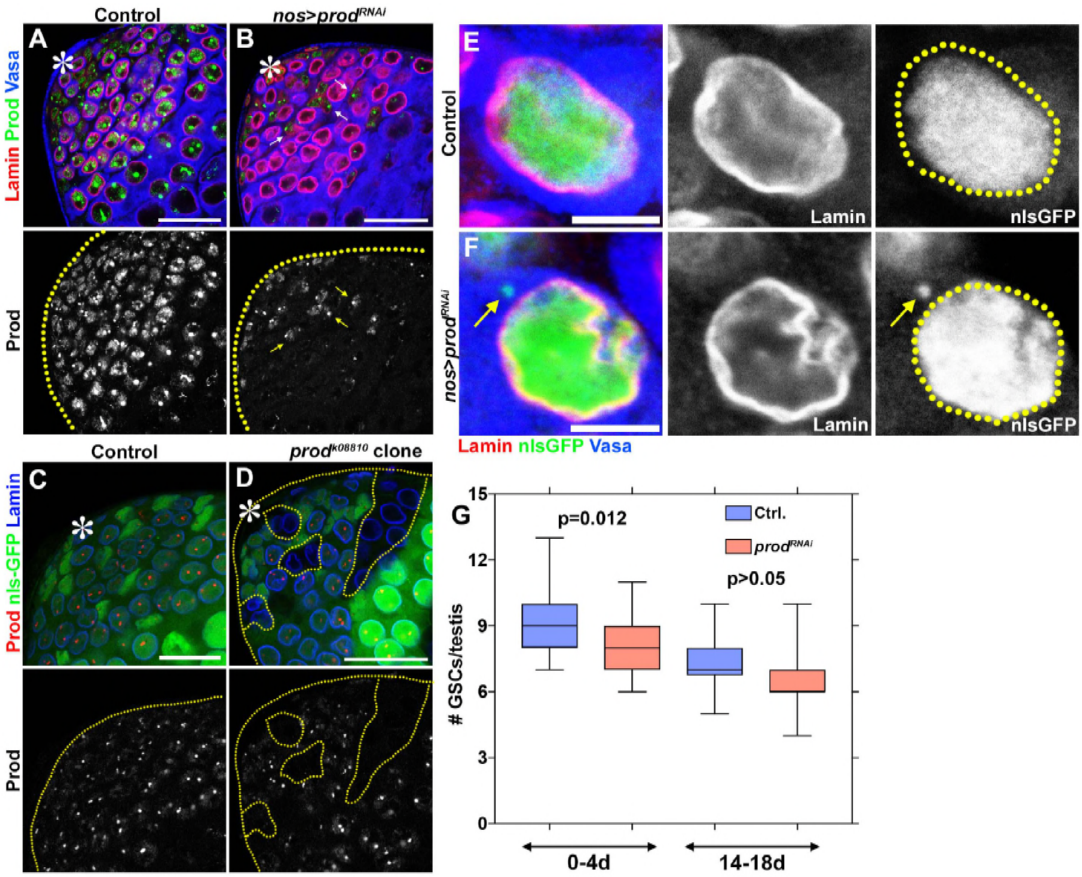

Figure 2 - figure supplement 1. Depletion of *prod* in spermatogonial cells does not result in micronuclei or loss of cellular viability. (A, B) Control (*nos-gal4*/+; *UAS-dcr-2*/+) (A) and *prod*-depleted (*nos-gal4*/*UAS-prod*^{RNAi}; *UAS-dcr-2*/+) (B) spermatogonial cells were stained with Lamin (red), Prod (green), and Vasa (blue). Arrows indicate cyst cells with Prod signal. Asterisk indicates the apical tip of the testis. Scale bars: 25μm. (C, D) Clones of control (heterozygous or wild-type) (C) or *prod*^{k08810} (D) were induced in spermatogonial cells and stained with Prod (red) and Lamin (blue). Yellow line indicates testis boundary and demarcates *prod*-null clones. Scale bars: 25μm. (E, F) Control (*nos-gal4*/+; *UAS-GFP-nls/UAS-dcr-2*) (E) and *prod*-depleted (*nos-gal4*/*UAS-prod*^{RNAi}; *UAS-GFP-nls/UAS-dcr-2*) (F) spermatogonial cells expressing nls-GFP (green) were stained with Lamin (red) and Vasa (blue). Arrow indicates nls-GFP in the cytoplasm of a *prod*-depleted spermatogonial cell. Scale bars: 5μm. (G) Box and whisker plot of the number of germline stem cells per testis across two time windows (control 0-4d n=26, *nos-*

gal4/*UAS-prod*^{RNAi} 0-4d n=50, control 14-18d n= 18, *nos-gal4*/*UAS-prod*^{RNAi} 14-18d n=39). P values from Student's t-test are shown.

Figure 2 – figure supplement 2

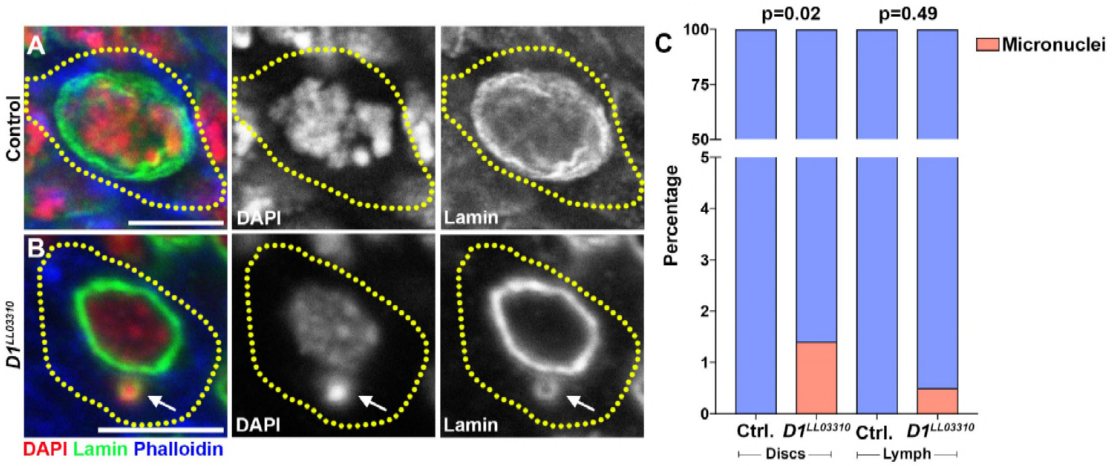

Figure 2 – figure supplement 2. Loss of *D1* results in low levels of micronuclei formation in larval imaginal discs and lymph glands. (A, B) Heterozygous control (A) and homozygous $D1^{LL03310}$ mutant (B) imaginal disc cells were stained with DAPI (red), Lamin (green), and Phalloidin (blue). Arrow indicates micronucleus. (C) Quantification of micronuclei containing cells in heterozygous control and homozygous $D1^{LL03310}$ mutant imaginal discs and lymph glands. Control discs n=360, *D1* mutant discs n=347, Control lymph n=215, *D1* mutant lymph n=210. P values from Fisher's exact test are shown. All scale bars are 5μm.

Figure 3

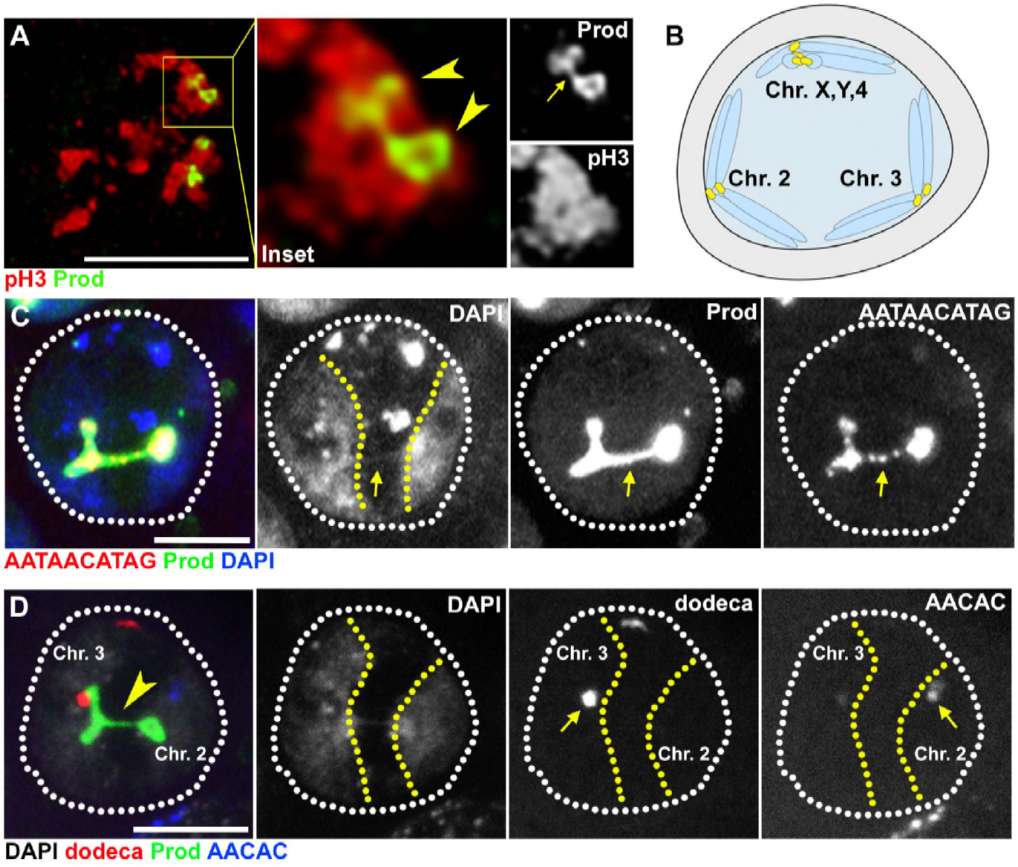

Figure 3. Prod bundles heterologous chromosomes through the {AATAACATAG}$_n$ satellite DNA. (A) Deconvolution microscopy of *Drosophila* larval neuroblasts in early prophase expressing GFP-Prod (green) under the control of *wor-gal4* and stained with pH3 (Ser10) (red). Arrowheads in the inset indicate two of the four Prod loci while the arrow indicates Prod threads connecting the two loci. (B) Schematic depicting how homologous chromosomes separate into distinct "territories" in spermatocytes in preparation of meiotic reductional division. One territory contains the X, Y, and 4th chromosomes, a second territory contains the 2nd chromosomes, and a third territory contains the 3rd chromosomes. (C) FISH against the {AATAACATAG}$_n$ satellite (red) in spermatocytes expressing GFP-Prod (green) under the control of *bam-gal4* and stained with DAPI (blue). Yellow line demarcates chromosome 2 and chromosome 3 territories. Arrow indicates chromatin thread linking the two territories that is positive for DAPI, Prod, and the {AATAACATAG}$_n$ satellite DNA. (D) FISH against the dodeca satellite (red) and the {AACAC}$_n$ satellite (blue) in spermatocytes GFP-Prod (green) under the

control of *bam-gal4* and stained with DAPI (white). Yellow line demarcates chromosome 2 and chromosome 3 territories. Arrowhead indicates chromatin thread linking the two territories that is positive for DAPI and Prod. Arrows indicate location of $\{AACAC\}_n$ satellite DNA that is specific to chromosome 2 and dodeca satellite DNA that is specific to chromosome 3. All scale bars are 5μm.

Figure 3 – figure supplement 1

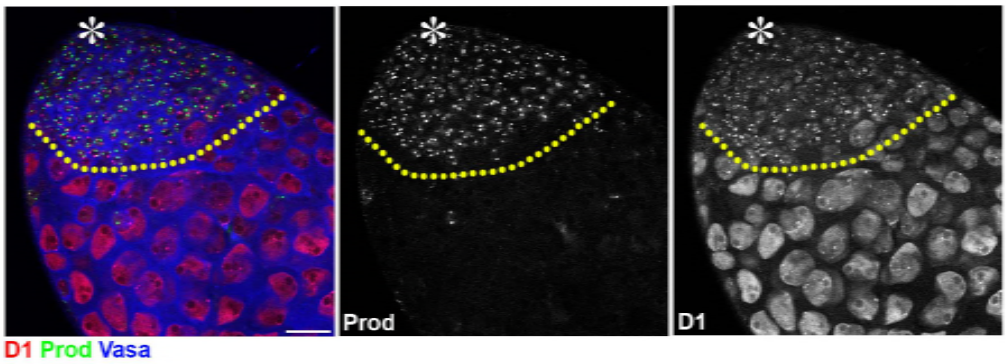

Figure 3 - figure supplement 1. Prod expression is not observed in *Drosophila* spermatocytes. The apical tip of a *Drosophila* testis is shown that was stained with D1 (red), Prod (green), and Vasa (blue). Asterisk indicates the apical tip. The yellow line separates spermatogonia from spermatocytes. Scale bar: 25μm.

Figure 4

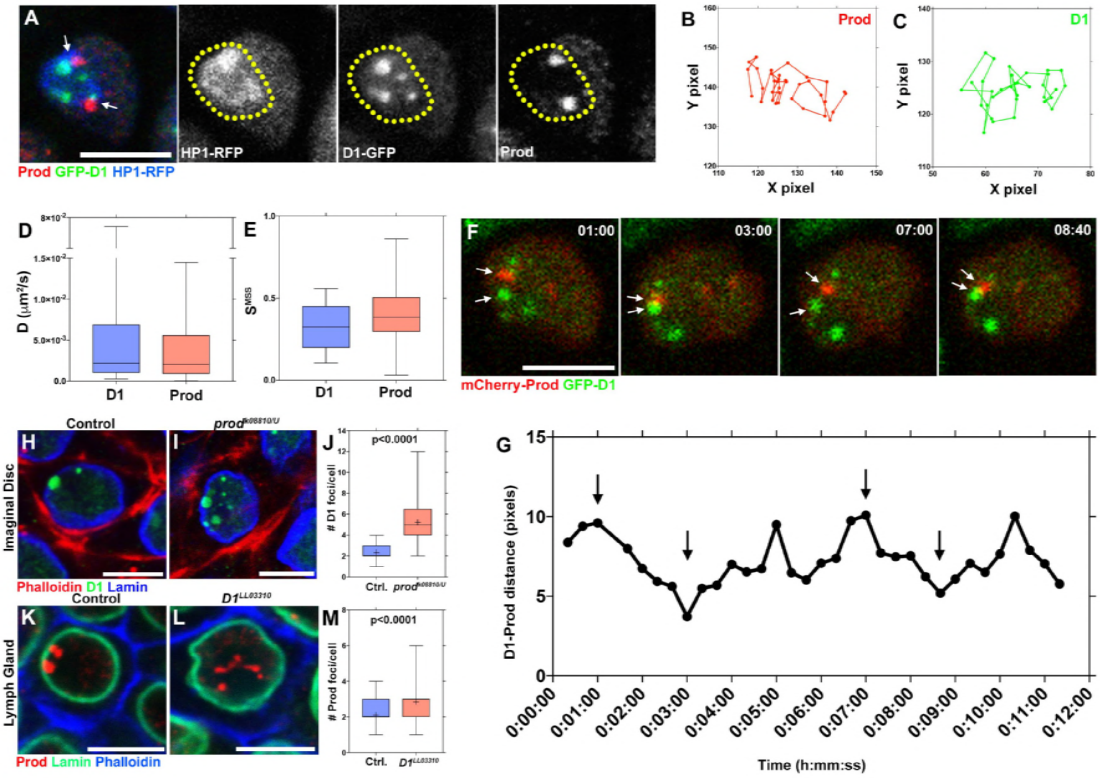

Figure 4. Dynamic interactions between D1 and Prod mediate the formation of chromocenters. (A) *Drosophila* lymph cells expressing D1-GFP (green) and HP1-RFP (blue) stained with Prod (red). Arrows indicate juxtaposed Prod and D1 foci. Yellow line demarcates the heterochromatic domain based on HP1 localization. Scale bar: 5μm. (B, C) Particle tracking analysis of single Prod (B) or D1 (C) foci in the XY plane. (D, E) Box-and-whisker plot of the diffusion co-efficients (D) and the slope of momentum scaling spectrum (E) of D1 (n=25) and Prod (n=29). (F) Time-lapse imaging of spermatogonia expressing *nos-gal4* driven UAS-mCherry-Prod (red) and D1-GFP (green). Arrows indicate Prod and D1 foci interacting in a "kiss-and-run" manner. Time is indicated in mm:ss. (G) Quantification of the distance between the D1 and Prod foci indicated in panel F over time. Arrows indicate the time points shown in panel F. (H, I) Heterozygous control (H) and $prod^{k08810/U}$ mutant (I) larval imaginal disc cells stained with Phalloidin (red), D1 (green), and Lamin (blue). (J) Box-and-whisker plot of the number of D1 foci per larval imaginal disc cell (control n=72 , $prod^{k08810/U}$ n=65). (K, L) Heterozygous control (K) and $D1^{LL03310}$ mutant (L) larval lymph gland cells stained with

Prod (red), Lamin (green), and Phalloidin (blue). (M) Box-and-whisker plot of the number of Prod foci per larval lymph gland cell (control n=63, $D1^{LL03310}$ n=66). All P values are from student's t-test. All middle bars: median. All crosshairs: mean. All scale bars: 5μm.

Figure 4 – figure supplement 1

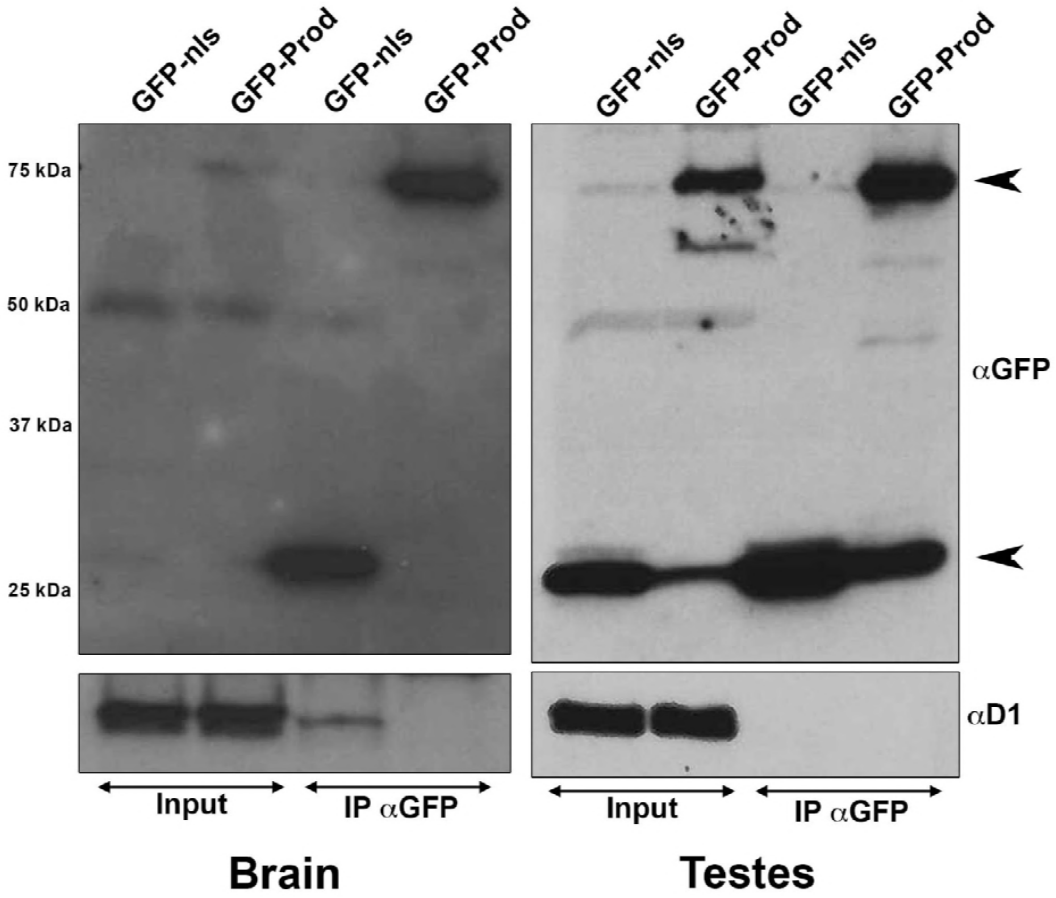

Figure 4 – figure supplement 1. Co-immunoprecipitation experiments from multiple tissue lysates did not detect an interaction between Prod and D1. (Left) Immunoprecipitation of GFP using GFP-Trap® magnetic beads from larval brains expressing UAS-GFP-nls or UAS-GFP-Prod under the control of *wor-gal4*. (Right) Immunoprecipitation of GFP using GFP-Trap® magnetic beads from Upd testis tumors expressing either UAS-GFP or UAS-GFP-Prod under the control of *nos-gal4*. Immunoprecipitated proteins were blotted using rabbit anti-GFP and guinea pig anti-D1. Expected sizes: GFP: 27kDa, GFP-Prod: 75kDa.

Figure 4 – figure supplement 2

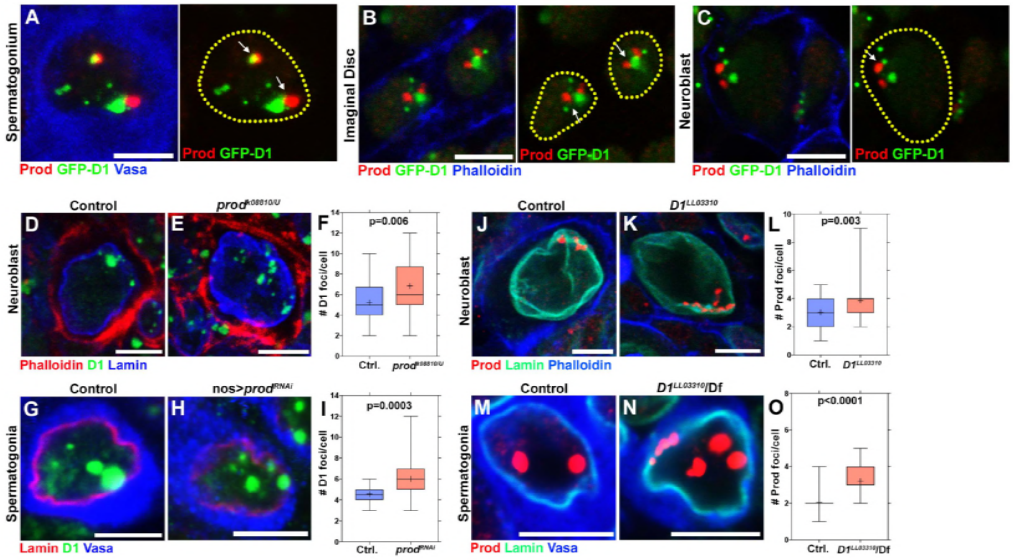

Figure 4 – figure supplement 2. Mutually dependent clustering of D1 and Prod in multiple cell types. (A) *Drosophila* spermatogonia expressing D1-GFP (green) and stained for Prod (red) and Vasa (blue). Arrows indicate D1 and Prod foci in close proximity to each other. (B, C) Larval imaginal disc cells (B) and neuroblasts (C) expressing D1-GFP (green) and stained for Prod (red) and Phalloidin (blue). Arrows indicate D1 and Prod foci in close proximity to each other. (D, E) Heterozygous control (D) and $prod^{k08810/U}$ mutant (E) larval neuroblasts stained with Phalloidin (red), D1 (green), and Lamin (blue). (F) Box-and-whisker plot of the number of D1 foci per neuroblast (control n= 32, $prod^{k08810/U}$ n=32). (J, K) Heterozygous control (J) and $D1^{LL03310}$ mutant (K) larval neuroblasts stained with Prod (red), Lamin (green) and Phalloidin (blue). (L) Box-and-whisker plot of the number of Prod foci per neuroblast (control n= 45, $D1^{LL03310}$ n=40). (G, H) Control (*nos-gal4*/+; *UAS-dcr-2*/+) (G) and *prod*-depleted (*nos-gal4*/*UAS-prod*^{RNAi}; *UAS-dcr-2*/+) (H) spermatogonia stained with Lamin (red), D1 (green), and Vasa (blue). (I) Box-and-whisker plot of the number of D1 foci per spermatogonial cell (control n=30 , *nos-gal4>UAS-prod*^{RNAi} n=30). (M, N) Heterozygous control (M) and $D1^{LL03310}$ mutant (N) spermatogonia stained with Prod (red), Lamin (green), and Vasa (blue). (O) Box-and-whisker plot of the number of Prod foci per spermatogonial cell (control n=75, $D1^{LL03310}$ n=75). All P values are from student's t-test. All crosshairs: mean. All scale bars: 5μm.

Figure 5

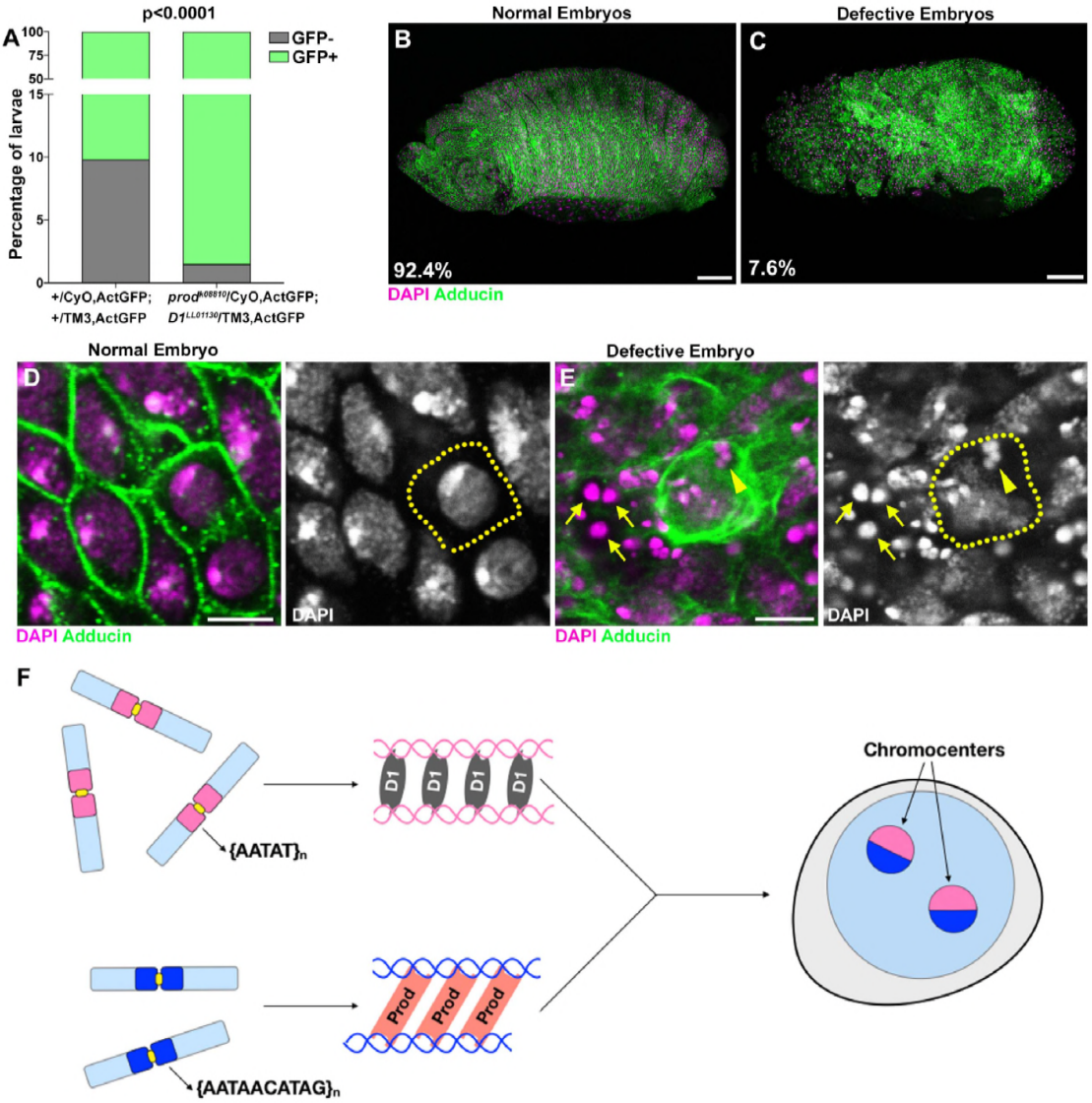

Figure 5. *D1 prod* double mutation leads to embryonic lethality. (A) Quantification of GFP-positive and GFP-negative first instar larvae sired by +/CyO, ActGFP; +/TM3, ActGFP and *prod*^{k08810}/CyO, ActGFP; *D1*^{LL03310}/TM3, ActGFP adults. GFP-negative larvae from +/CyO, ActGFP; +/TM3, ActGFP parents are wild type while GFP-negative larvae from *prod*^{k08810}/CyO, ActGFP; *D1*^{LL03310}/TM3, ActGFP parents are double mutants. P value from student's t-test is shown. (B, C) Normal (B) and defective (C) embryos from *prod*^{k08810}/CyO, ActGFP; *D1*^{LL03310}/TM3, ActGFP are stained with DAPI (red) and Adducin (green). Percentage of normal and defective embryos are indicated from n=132. Scale bars: 25μm. (D, E) Close-up view of normal (D) and

defective (E) embryos from (B, C). Yellow line indicates cell boundary based on adducin staining. Arrows indicate extra-nuclear DNA and the arrowhead indicates micronuclei. Scale bar: 5μm. (F) A model depicting the modular architecture of chromocenters in Drosophila *melanogaster*. Modules of D1-$\{AATAT\}_n$ and Prod-$\{AATAACATAG\}_n$ interact dynamically to bundle the entire chromosome complement into chromocenters.